JOURNAL OF AIRCRAFT
Vol. 42, No. 5, September–October 2005

Discrete-Blade, Navier–Stokes Computational Fluid Dynamics Analysis of Ducted-Fan Flow

Gene C. Ruzicka* and Roger C. Strawn†
NASA Ames Research Center, Moffet Field, California 94035-1000
and
Edward T. Meadowcroft‡
The Boeing Company, Ridley Park, Pennsylvania 19142

The application of overset grid methods to studying the flowfield of the FANTAIL™ antitorque system of the RAH-66 rotorcraft is described. The FANTAIL itself and the experimental program used to design it are described first. Then, OVERFLOW-D, an overset grid-based, Navier–Stokes computational fluid dynamics code is reviewed, and its adaptation to the ducted fan geometry of the FANTAIL is explained. The modeling of the FANTAIL using OVERFLOW-D, including grids and boundary conditions, is explained in detail. The results of numerical studies of the hovering FANTAIL are presented and are shown to compare well with experiment. Flowfield visualizations are presented and are used to explain how the blade tip vortices combine with the adverse pressure gradient beneath the rotor disk to impact flow along the duct wall beneath the disk.

Nomenclature

C_Q	=	rotor torque coefficient
$C_{Q\text{ref}}$	=	computed rotor torque coefficient at 38-deg collective
C_T	=	rotor thrust coefficient
$C_{T\text{ref}}$	=	computed rotor thrust coefficient at 38-deg collective
c_l	=	blade section lift coefficient
c_p	=	pressure coefficient with respect to blade tip speed
Q	=	rotor torque
R	=	rotor radius
T	=	rotor thrust
t	=	time
u, v, w	=	Cartesian fluid velocity measures
x, y, z	=	Cartesian body axes
ρ	=	density of air
Ω	=	rotor angular velocity

I. Introduction

DUCTED fans are highly efficient and versatile propulsion devices. Their use in rotorcraft antitorque systems dates back to the fenestron, that is, fan in fin, of the Aerospatiale SA-341 of 1969, and a similar device, the FANTAIL™ of the Boeing–Sikorsky RAH-66, is the subject of this study.

The most often-cited advantage of a ducted fan over an isolated rotor is its efficiency, which results from two benefits of the surrounding duct wall: First, the duct wall itself makes a significant contribution to the ducted-fan thrust. Second, the duct mitigates blade lift losses by suppressing the escape of air around the blades' ends. However, for a rotorcraft antitorque system, the key advantages of a ducted fan are its robustness and maintainability, although the protection that the surrounding duct offers ground personnel from the (essentially invisible) spinning rotor blades is another important benefit.

Unfortunately, the utility of a ducted fan is matched by the difficulty of analyzing its aerodynamics. The most readily apparent problem is the perhaps unique complexity of the ducted fan's geometry, which consists of multiple, heterogeneous surfaces, some of which are rotating and others of which are fixed. There are also more familiar, but no less formidable, aerodynamic and computational issues to contend with. Separation of the flow from the surrounding duct wall plays a key role in the development of lift, and so Navier–Stokes simulations, along with their attendant high-resolution grids, must be employed on the duct wall as well as on the blades. Ducted-fan flows are highly vortical, and computational fluid dynamics (CFD) analyses must, therefore, confront the ever-daunting problem of spurious numerical dissipation of the vortex wake. In view of these difficulties, devising accurate, reliable tools to analyze ducted-fan aerodynamics constitutes an ongoing, major challenge.

Although CFD-based methods have been used in ducted-fan studies,[1,2] most of these studies employ simplified rotor aerodynamic models, such as pressure-disk models, to reduce the size of the model and otherwise simplify the analysis. Although these simplified models are quite satisfactory for computing interference effects, or for predicting the overall behavior of the ducted fan, they provide, at best, azimuth-averaged approximations to flow within the duct. Therefore, they may miss critical flow features, especially in regions close to the blades; indeed, rotorcraft aerodynamicists have long been aware of these same shortcomings in actuator-disk rotor models, which are often used in non-CFD rotorcraft analyses. Employing complete, three-dimensional CFD models of the discrete blades is a way to overcome these modeling shortcomings, at the expense of lengthier, costlier computations, and overset grid methods offer a means to incorporate such models into CFD analyses.

Overset grids employ multiple, structured grids that overlap at their boundaries. Quite complex flow domains may be readily modeled by combining overset grids, subject to the requirements of compatible mesh sizing and sufficient overlap at the grid interfaces. By the mere overlapping of the grids rather than pointwise connection, the method neatly circumvents the problem of generating structured grids that match pointwise along complex boundaries and simplifies the problem of matching solutions obtained from different grid systems at connecting points. The individual grids can be integrated implicitly, and, although intergrid updating is explicit, experience has shown that sizable time steps can be employed without loss of computational stability. Thus, overset grid methods combine

Presented as Paper 2004-0048 at the AIAA 42nd Aerospace Sciences Meeting and Exhibit, Reno, NV, 5–8 January 2004; received 2 March 2004; accepted for publication 13 December 2004.

*Aerospace Engineer, U.S. Army/NASA Rotorcraft Division, Aeroflightdynamics Directorate, Mail Stop N258-1.
†Group Leader, U.S. Army/NASA Rotorcraft Division, Aeroflightdynamics Directorate, Mail Stop N258-1. Associate Fellow AIAA.
‡Aerospace Engineer, Boeing U.S. Army Programs and Military Rotorcraft.

the ability of unstructured flow solvers to handle complex geometries, with the lower computational costs of structured flow solvers. Overset grid methods have been successfully applied to rotating-blade flows[3,4] and, therefore, are obvious candidates for modeling ducted-fan aerodynamics.

The design of the FANTAIL was based on an extensive experimental program,[5] a fortuitous dividend of which is a valuable database for validating computational tools for studying ducted fans. In this paper, progress in applying the overset grid flow solver OVERFLOW-D to analyzing FANTAIL aerodynamics is discussed, and the code is validated against experimental data. This study is particularly timely in view of the rising importance of ducted fans in aviation, as evidenced by their key roles in several recent, innovative vehicles, particularly unmanned aerial vehicles. Moreover, it is felt that the results of this study will be relevant to the analysis of turbomachinery; indeed, some of the analytical techniques employed in this study originated in turbomachinery research, and a glance at contemporary turbomachinery literature[6] clearly reveals the close relationship of ducted-fan and turbomachinery flows.

The paper begins by describing the FANTAIL and the experimental study used to design it. Then, the OVERFLOW-D flow solver is described, with a special emphasis on adapting it to the modeling of ducted fans. Next, the OVERFLOW-D computational model of the FANTAIL is described, and the flowfield solutions are presented and compared with experimental results. Finally, the study's conclusions are presented.

II. FANTAIL Design and Evaluation

A. Introduction

The RAH-66, also known as the Comanche, is an armed reconnaissance and light attack helicopter designed for air combat and nap-of-Earth operations in day, night, and adverse weather conditions. The FANTAIL antitorque system employs a fan-in-fin configuration similar to the Sikorsky S-67 Blackhawk fin-in-fin flown in 1974 and the Aerospatiale fenestron.[7] Compared to conventional tail rotors, the FANTAIL has superior survivability characteristics. In addition, the FANTAIL requires less power to hover than conventional tail rotors with similar disk loadings. The FANTAIL configuration was developed in a series of wind-tunnel tests, including two-dimensional airfoil tests: a one-third-scale test of the FANTAIL inlet and exhaust lip radii; a one-quarter-scale powered model of the complete helicopter configuration, including interaction effects of the fuselage and main rotor on the FANTAIL and empennage; three-quarter-scale and full-scale powered tests of the FANTAIL; and, finally, the H-76 FANTAIL Demonstrator flight test. These data were combined with simulation studies, S-67 test data, and analyses during the trade studies to refine the FANTAIL design.

B. FANTAIL Design

The FANTAIL is an eight-bladed rotor with a rectangular planform, NACA 64 series airfoils, and −7 deg of twist from hub to tip. The 64-series airfoils provide the required aerodynamic characteristics over the design envelope while minimizing development risk. The −7-deg twist provides optimal performance while maximizing responsiveness as the rotor transitions from negative to positive collectives. The untapered planform minimizes manufacturing risk. The number of blades is considered optimal for acoustics and durability. The fan tip speed is based on acoustics. Fan solidity was chosen based on performance and the turn to target manuever requirement.

The FANTAIL duct is critical to achieving high-performance efficiency. In hover, the duct allows the fan diameter to be smaller than a conventional tail rotor for the same power required. Negative static pressure on the duct inlet produces approximately 50% of the FANTAIL thrust. The duct depth has been optimized for hover and forward flight. The duct depth was selected to maximize hover performance while minimizing profile drag in forward flight. The final duct configuration is the minimum depth required to house the support structure and achieve acoustics goals. The duct divergence angle of 5 deg (half-angle) was chosen to prevent premature flow separation along the wall and to achieve performance goals. A sharp exit radius at the duct outlet was required for best static performance, but negative thrust and forward flight performance were compromised.

C. FANTAIL Test Program

Three-quarter-scale wind-tunnel[8] and full-scale whirl-tower tests[9] were used in the test program. Although these tests were performed on different models at different scales in different test facilities, the aerodynamic performance data in the two tests are nearly identical.

1. Three-Quarter-Scale Wind-Tunnel Test Description

The three-quarter-scale wind-tunnel test 1 was conducted in the Boeing vertical takeoff and landing wind tunnel (BVWT) from July–November 1989. The purpose of this test was to determine aerodynamic and acoustic characteristics of the FANTAIL antitorque device as well as its tail and closure configurations on a nearly full-scale FANTAIL design to minimize scaling requirements. The main test objectives were to 1) obtain performance and loads characteristics of the FANTAIL during hover, low-speed, quartering, sideward, and rearward flight and high-speed forward flight; 2) determine aerodynamic characteristics, both with tail on and off; 3) quantify fan fairing and momentum drag; 4) establish control derivatives and control power; 5) determine fan dynamic characteristics; and 6) determine fan acoustic characteristics.

The BVWT is a closed-circuit, single-return wind tunnel capable of airspeeds over 200 kn. The test section has a 20 by 20 ft cross section with solid walls. The test section walls and floor can be removed for hover testing. During hover testing, the model was yawed 110 deg in the left sideward flight direction, allowing the fan wake to blow in the upstream direction. The north wall (left side, Fig. 1) and roof were removed, and the south wall and floor were left in the test section.

The test model was a 75%-scale model consisting of a tailboom, fan, fan gearbox, slipring, fan duct and shrouds, canted vertical tail, and a high-mounted horizontal tail. The fan tip speed was equal to its full-scale magnitude. The blade twist schedule was the same as full scale. The blade thickness and taper differed from full scale. The blade tip to duct clearance was 80% of the full-scale clearance. A strain-gauged six-component balance measured total forces of the entire model. The gauge time stream data are processed for the mean, minimum, and maximum unsteady values. A nose fairing covered the balance and drive shafting. The nose fairing was attached to the ground side of the balance. A gap existed between the grounded nose and the shroud on the live side of the balance. Flex couplings were installed in the drive shaft and strain gauged to measure torque. To improve accuracy, a torque bridge was added to the drive shaft near the ground end of the balance.

Many pressure taps were installed throughout the model fairings, mainly on the inlet side duct lips and the vertical tail. A limited set

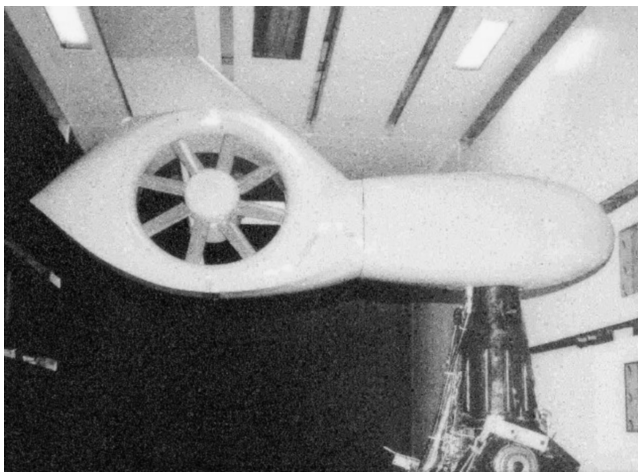

Fig. 1 BVWT test model.

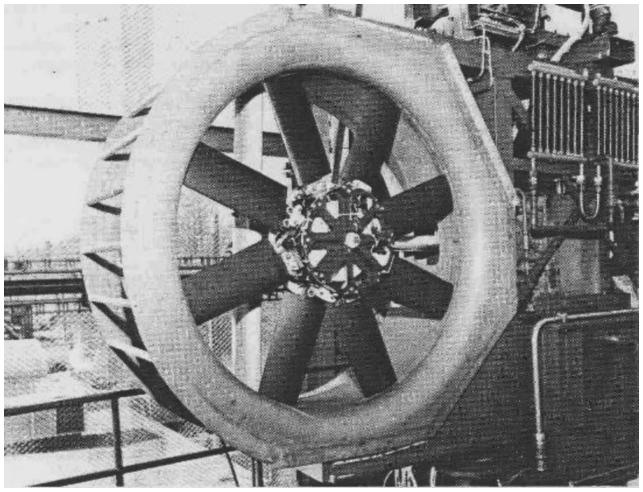

Fig. 2 Whirl-tower test model.

of pressure taps were installed on the exhaust side. Pressure measurements were taken with a Pressure Systems, Inc.-type apparatus consisting of pressure taps connected to small-diameter air tubes, which were connected to individual transducers in a base module. An algorithm converted the pressure measurements into derived shroud fairing thrust. Isolated fan-alone thrust was derived from balance-measured total system thrust minus pressure-derived shroud thrust.

2. Full-Scale Hover Whirl-Tower Test

The full-scale hover whirl-tower test (Fig. 2) was conducted at the Sikorsky Aircraft 2000 HP tail rotor precession test stand from June 1995 to January 1996. The purposes of the FANTAIL whirl-tower test were to 1) demonstrate functional adequacy, structural integrity, and airworthiness of the FANTAIL before first flight; 2) obtain aerodynamic hover performance data at various tip Mach numbers; 3) define the blade to duct clearance, which is is measured using a blade at flat pitch at the 50% blade chord; and 4) evaluate overall noise signature of the fan in the far acoustic field. The test article was a complete full-scale FANTAIL rotor/gearbox and shroud assembly. None of the vertical and horizontal tail was assembled.

All performance testing was conducted with the FANTAIL tip path plane oriented parallel to freestream winds. All struts and fairings (including gearbox, gearbox support struts, spinner, and driveshaft cover) in the duct were installed. Torque was measured at the test facility gearbox output shaft. System (fan and shroud) thrust was measured by a load cell in the test facility. An array of pressure taps was installed on the inlet side duct lips. Pressure transducers were used to measure the vacuum pressure at small holes in the duct. An algorithm multiplying the pressure measurements by weighted surface areas derived shroud thrust. The algorithm assumes that ambient pressure prevails beneath the rotor disk. Isolated fan-alone thrust is derived as total system thrust minus derived shroud thrust. The three-quarter and whirl-tower tests were performed on different models at different scales in different test facilities, yet the aerodynamic performance data between the two tests are almost identical. When CFD is compared to test data, usually the results from only one of the tests is presented.

III. OVERFLOW-D Flow Solver

A. Overview

The computations for this paper use the Reynolds-averaged Navier–Stokes flow solver, OVERFLOW-D. OVERFLOW-D is based on NASA's OVERFLOW Navier–Stokes solver,[10] with added capabilities for the modeling of rigid bodies in relative motion and for efficient execution on parallel computers. Solutions are computed on structured, overset grids with body-conforming grids for the near field and uniform Cartesian off-body grids for the far field. Earlier studies contain details on the application of OVERFLOW-D to an isolated conventional rotor in hover[3] and demonstrate its application to isolated tilt rotors.[4] Both Refs. 3 and 4 contain details on grid generation, code setup, and interpretation of results. They demonstrate the code's ability to match experimentally measured figures of merit to within 2%. The main complication for the FANTAIL is the close proximity of the shroud to the rotor system. The relative motion between the rotor blades and the shroud wall presents additional issues for grid generation and algorithm formulation that are addressed in the following sections.

B. Rotational Grid Motion

Hovering rotor simulations can take advantage of the fact that the flowfield is steady when viewed from a blade-fixed frame of reference. The calculations in this paper use a formulation originally developed by Holmes and Tong[11] for turbomachinery and later applied by Chen et al.[12] to rotorcraft to convert the rotating-blade Navier–Stokes equations to a steady-state problem. Steady-state solutions require much less computational effort than their time-accurate counterparts, which makes it feasible to use larger grids to better capture the details of the flowfield, especially the rotor wake in hover. The resulting Navier–Stokes equations for a hovering rotor blade are

$$\frac{\partial \boldsymbol{Q}}{\partial t} + E(\boldsymbol{Q}) = V(\boldsymbol{Q}) + R(\boldsymbol{Q}) \tag{1}$$

where $\boldsymbol{Q} = [\rho, \rho u, \rho v, \rho w, \rho e]$ is the solution vector of conservative variables, $E(\boldsymbol{Q}) = \partial E_i / \partial x_i$ is the convective operator, $V(\boldsymbol{Q}) = \partial V_i / \partial x_i$ is the thin-layer viscous operator, and $R(\boldsymbol{Q}) = [0, \rho v \Omega, -\rho u \Omega, 0, 0]$ is the z-coordinate rotational source term. Although the computational formulation in Eq. (1) has often been used to compute steady solutions for isolated rotor systems, one important question is whether or not it is possible to use that formulation to compute a steady-state solution for the combined rotor and shroud. The complication here is that there is relative motion between the rotor and the stationary shroud. To answer this question, recall that the formulation in Eq. (1) models a steady-state problem where the computational grid rotates at a constant angular velocity. However, even though the grid rotates, the solution vector $\boldsymbol{Q}$ is still referenced to the inertial frame, and that circumstance, combined with the axisymmetry of the shroud, makes it possible to enforce simultaneously the inertial-system no-slip viscous boundary condition on the surface of the shroud. The resulting computational model correctly reflects the relative motion between the rotor and shroud while preserving the steady-state nature of the problem.

The existence of a steady-state solution is perhaps more readily grasped with the aid of Fig. 3. Figure 3 shows a complete ducted fan at arbitrary times $t = t_1$ and $t = t_2$; for simplicity, Fig. 3 shows a four-bladed fan rather than an eight-bladed fan. The flowfield will admit a steady-state solution if it can be demonstrated that neither the governing equations nor the boundary conditions have explicit time dependencies. Clearly, Eq. (1) has no explicit time dependencies. Now, consider the boundary conditions, starting with the blades. Because the blades are viscous and the velocities are defined with respect to the inertia frame, the velocity at each point on the surface of the blade grid is $\boldsymbol{v} = \boldsymbol{\Omega} \times \boldsymbol{r}$ where $\boldsymbol{r}$ is the position vector from the

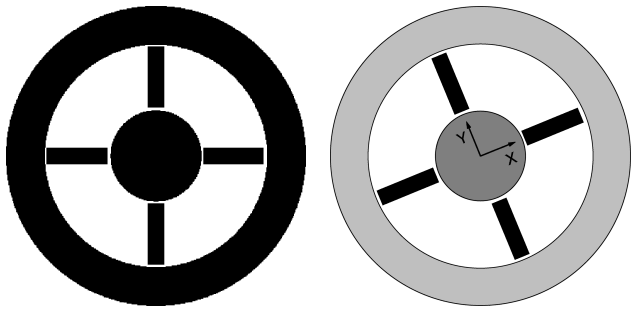

a) b)

Fig. 3 Ducted fan with axisymmetric shroud at times a) $t = t_1$ and b) $t = t_2$.

spin axis to the point on the blade's surface. This expression is valid for all time and is independent of time for the grid coordinate system, which rotates with the blade. Similarly, the inviscid hub boundary condition, $\boldsymbol{v}_n = 0$, where $\boldsymbol{v}_n$ is the velocity normal to the hub surface, will hold for all time at each point on the hub. Finally, consider the boundary conditions on the shroud. Let the surface of the shroud be defined by the equation $f_{\text{shroud}}(x, y, z) = 0$ at time $t = t_1$, where x, y, and z are referred to the rotating coordinate system. Then, the boundary condition of a point on the shroud at $t = t_1$ is evidently $\boldsymbol{v} = 0$ for any point satisfying $f_{\text{shroud}}(x, y, z) = 0$. It is apparent from Fig. 3 that at any subsequent time $t = t_2$, the shroud's surface will continue to be defined by the equation $f_{\text{shroud}}(x, y, z) = 0$ because of the shroud's axisymmetry, and, consequently, the homogeneous boundary condition applicable at $t = t_1$, which has no time dependencies, will apply for all time. Thus, neither the flowfield's equations nor its boundary conditions have explicit time dependencies.

Confusion among some about the existence of a steady solution seems to stem from the fact that a shroud surface point with coordinates x, y, and z fixed in the rotating coordinate system refers to different points at different times on the fixed shroud surface, which would appear to introduce a time dependency into the problem. However, this consideration is inherently irrelevant in an Eulerian description of the problem, which examines the behavior of fluid particles at their instantaneous positions.

The foregoing analysis shows that a key requirement for the existence of a steady solution is the axisymmetry of the shroud. If the shroud merely has n-fold periodicity like the blades, rather than being fully axisymmetric, then the viscous shroud boundary conditions will exhibit an explicit time dependency, and a steady-state solution will not exist.

C. Periodicity

The solution's n-fold azimuthal periodicity makes it possible to truncate the model to size $1/n$ of the complete system, with the omitted region replaced by periodic boundary conditions on the azimuthal boundaries. Thus, periodicity allows for significant computational savings; for example, a four-bladed rotor system only requires one-quarter of the grid points that are needed to model the complete rotor system. The implementation of periodicity in OVERFLOW-D uses two layers of ghost cells that extend beyond each of the periodic inflow and periodic outflow boundaries. These ghost cells match point to point with counterparts in the interior of the computational domain on the opposite periodic boundary. The exterior ghost cells are updated from their interior, periodic counterparts following each iteration of the flow solver after the velocity vector is rotated by $+90$ or -90 deg, thereby enforcing the azimuthal periodicity of the flow.

IV. FANTAIL Computational Model

A. Overview

The numerical studies are based on the simplified FANTAIL geometry shown in Fig. 4. Note that all of the empennages have been removed, leaving behind an axisymmetric duct wall. Note that the simplified model satisfies all of the requirements for steady flow, and a quadrant model of the flow domain is used for the analysis. In principle, an octant model could be employed because of the eightfold periodicity, but that would require explicitly generating the model's wedge-shaped off-body grids, whereas a quadrant model exploits OVERFLOW-D's capability for generating Cartesian, off-body grids. In the discussion that follows, all units are dimensionless, with length dimensions normalized to the rotor radius.

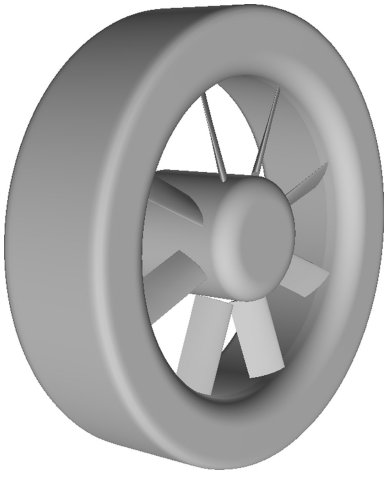

Fig. 4 Idealized FANTAIL geometry.

B. Near-Body Grids

1. Grid Geometry

As is usually done in overset grid-based flow simulations, two sets of grids are employed. The first set are near-body grids, which are shown in Fig. 5. These are body-fitted curvilinear grids located near the flow domain boundary surfaces, which are the blades, the hub, and the shroud. These grids have generally high resolution, and their purpose is to resolve sharp flow gradients arising from abrupt geometry changes, or from boundary layers, in the vicinity of the solid boundaries they are fitted to.

The fitted cap grids around the blades' ends are needed to satisfy the no-flow boundary conditions at those locations. Observe that the blades are truncated before reaching the hub, thereby introducing artificial gaps between the blade root ends and the hub. Truncating the blades in this fashion allows the grids to be modified for changes in collective angle by simply rotating the grids about the blade pitch axis, which greatly simplifies grid generation.

The rectangles on the shroud in Fig. 5 are regions where the shroud grids must be refined significantly because of their close proximity to the blades' tips. Apart from the complex aerodynamic phenomena expected near isolated blade tips, the presence of the nearby wall is likely to contribute further to sharp flow gradients because of the abrupt change in geometry where the shroud and the blades meet and from the steep change in velocity across the narrow gap between the blade and shroud surfaces. Figure 6 illustrates shroud grid refinement in the vicinity of the blades' tips. Additional details of the near-body grids and the innermost off-body grids are shown in Fig. 7, which shows a slice through the grid system normal to the duct axis at blade level.

2. Boundary Conditions

Viscous, that is, no-slip, surface boundary conditions are used on the solid surfaces of the blade and shroud grids. Because fluid velocities near the hub are generally low and the FANTAIL flowfield

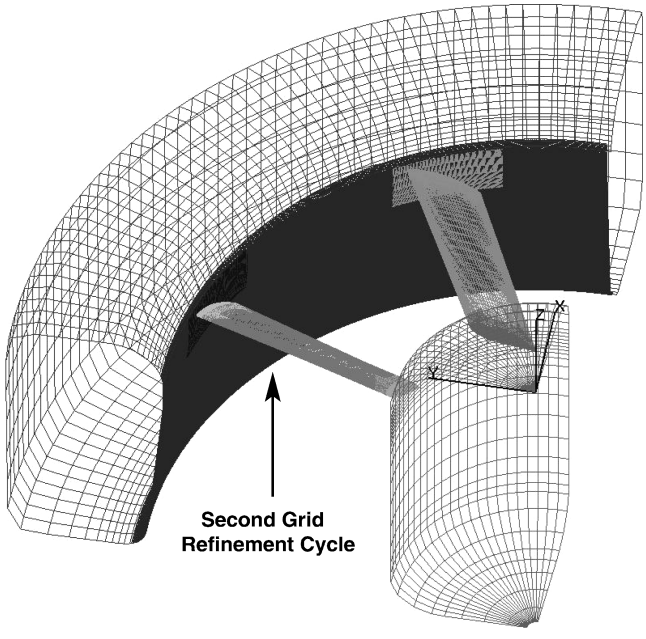

Fig. 5 Near-body grids, quadrant FANTAIL CFD model.

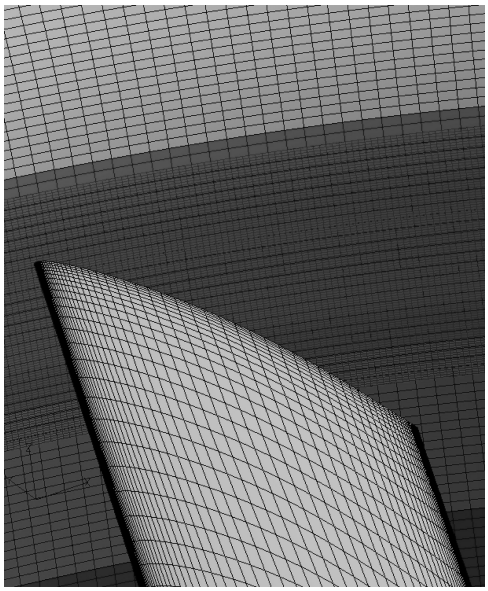

Fig. 6 Refined shroud grid.

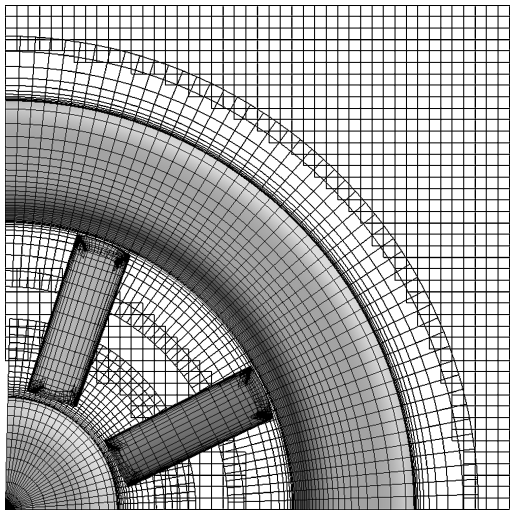

Fig. 7 Grids at blade elevation.

is not expected to be sensitive to conditions in that vicinity, the hub surface is treated as inviscid to eliminate the need for a high-resolution, viscous grid. Periodic boundary conditions are applied to the azimuthal ends of the hub and shroud grids as described earlier.

C. Off-Body Grids

1. Grid Geometry

The off-body grids, as their name implies, are generally farther away from the bounding surfaces of the flow domain, and, because they occupy regions where flow gradients are likely to be smaller, they can be made coarser and can be Cartesian in structure, which simplifies computations.

The off-body grid system used in the study (Fig. 8) extend nine rotor radii from the origin in all three directions. The grids are arranged in four concentric layers, with the grid spacing of each double that of the one beneath, starting with a spacing of 0.02.

2. Boundary Conditions

The off-body grids are subject to the same periodicity requirements as the near-body grids, and, accordingly, periodic boundary conditions are applied to points on the periodic planes $x = 0$ and $y = 0$ (Fig. 8). All of the remaining exterior boundaries of the off-body grids are on the exterior of the computational domain, and, as is generally the case in CFD computations, characteristic boundary conditions based on Riemann invariants are applied at these boundaries. In hover calculations, where there is no sideflight, it is also helpful to embed source-sink pairs in the flowfield to ensure that rotor downwash is exhausted from the flow domain instead of being reflected off of the exterior boundaries and recirculated back into the flow.[12]

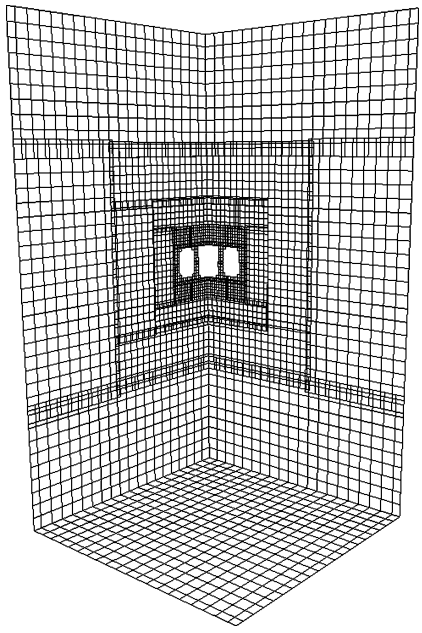

Fig. 8 Off-body grids.

D. Sealed-Gap Configuration

It is sometimes helpful to interpret the results, both experimental and computed, by comparing them with a companion analysis in which the blade–shroud gap sealed. The sealed gap geometry was obtained from the baseline geometry by replacing the tip cap grids with collar grids that wrapped around the blades' tips and shroud, thereby sealing off the gaps. The shroud in the companion analysis had to be viscous and rotating (instead of nonrotating) to have kinematic compatibility with the blades at the shroud–blade junction: This point is further explained shortly. Because the shroud in the actual FANTAIL is nonrotating, the sealed-gap configuration cannot be regarded as a limiting case of a finite-gap configuration, but the two models still have much in common, and, as will be seen later, comparing the finite-gap and sealed-gap configurations helps to understand how the gap influences the flowfield.

Note that it is not physically possible to have a sealed-gap ducted fan with the shroud fixed and viscous and the blades spinning and viscous. The reason this configuration is unrealizable is that a fluid particle at a blade–shroud juncture would have to be simultaneously spinning and fixed because of its placement on a viscous blade surface and on the viscous shroud surface: Clearly, the particle cannot possibly be both. Hence, it was necessary to alter the sealed-gap boundary conditions as explained earlier to obtain a mathematically well-posed problem.

V. Numerical Results

A. Overview

The numerical studies computed steady-state solutions for a hovering FANTAIL with blade collective angles of 8, 18, 28, and 38 deg. Unless otherwise noted, all solutions are for the finite blade–shroud gap configuration.

All computations were performed on the IBM SP4 computer at the U.S. Naval Oceanographic Office at NASA Marshall Spaceflight Research Center. Each simulation required about 20,000 time steps

Table 1 Grid dimensions, first grid refinement cycle

Grid	Coarse grid	Refined 1 grid
Blades	$2 \times (123 \times 34 \times 51) = 426{,}564$	$2 \times (\mathbf{203} \times 40 \times 66) = 1{,}071{,}840$
Tip caps	$2 \times (53 \times 45 \times 52) = 243{,}360$	$2 \times (\mathbf{148} \times \mathbf{79} \times 59) = 1{,}379{,}656$
Root caps	$2 \times (82 \times 57 \times 50) = 467{,}400$	$2 \times (82 \times 73 \times 63) = 754{,}236$
Hub	$111 \times 72 \times 30 = 239{,}760$	$111 \times 72 \times 40 = 319{,}680$
Shroud	$256 \times 146 \times 30 = 1{,}121{,}280$	$271 \times 152 \times 56 = 2{,}306{,}752$
Shroud patches		$2 \times (101 \times 85 \times 44) = 755{,}480$
Total near body	2,503,044	6,557,292
Off body	3,687,086	3,687,086
Total	6,190,130	10,274,730

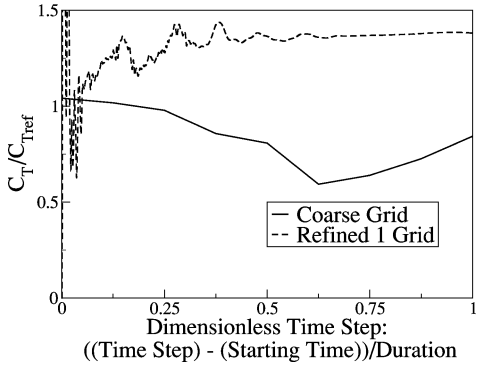

Fig. 9 OVERFLOW-D solution convergence for coarse and baseline grids, hover, 28-deg collective.

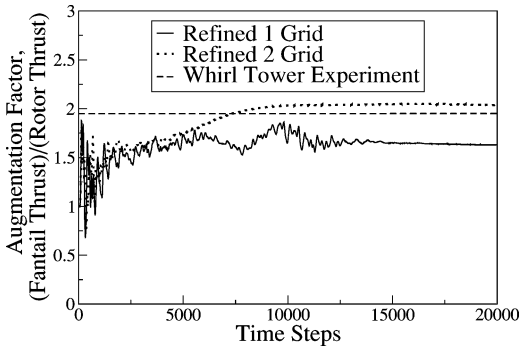

Fig. 10 OVERFLOW-D FANTAIL augmentation factor with refined grids, 38-deg collective, hover.

to reach a steady-state solution and required a cumulative 400 CPU h spread across 16 processors. The parallel processing efficiency was typically about 85%.

B. First Grid Refinement Cycle: Convergence Issues

To obtain a CFD solution that agrees well with experiment, two cycles of grid refinement were needed. At first, the computed solutions were highly unsteady, which seemed inconsistent with the experimental data and with reports from observers of the experiments, even after allowing for the fact that the balance-mounted experimental aparatus would have filtered out unsteadiness to some degree. It was, therefore, concluded that the unsteadiness was caused by numerical error, and the study's early focus was on obtaining a converged, steady solution.

The regions of the flow that seemed the most likely source of numerical unsteadiness were 1) near the duct outlet, because of the potential for flow separation from the duct wall and 2) near the blades' tips, because of the complex flow phenomena occurring there. A companion sealed-gap analysis readily produced a steady solution, which suggested that the cause of the unsteadiness was not separation of the flow from the shroud outlet; therefore, the next step was to try refining the blade grids to better resolve the flow in the blade tip regions.

In Table 1, the dimensions of the coarse grid, which was initially used in the study and which gave an unsteady solution, is compared with the refined 1 grid, which first gave a steady, converged solution. The grid dimensions give the number of points in the three curvilinear coordinate directions of each subgrid; following the usual convention for describing structured grids, the dimensions are given in the order of cross section, span, and outward directions. The refined 1 grid is actually the result of several refinement steps, and the boldfaced numbers in Table 1 indicate the grid dimensions that proved crucial in producing the converged solution. Note that the shroud patches were not employed in the original coarse grid and were found to be helpful, but of secondary importance, in stablizing the solution.

The properties of the solutions are illustrated in Fig. 9, which shows the total FANTAIL thrust vs time steps. Note that the thrust produced by the refined grid is both steadier and larger than in the coarse grid solution. These results are consistent with a rule of thumb for OVERFLOW-D analyses that a minimum of about 200 points are required around an airfoil cross section to develop an accurate solution. However, it is rather anomalous for grid refinement to stabilize a solution; typically, grid coarsening benefits solution stability by increasing the spurious numerical dissipation in the grid. The reasons for this anomaly are not fully understood, but one possible explanation is that some critical flow feature is not getting adequately resolved in the coarser grid, and its absence forces the flow to become unsteady.

C. Second Grid Refinement Cycle: Augmentation Factor Accuracy

Although the first grid refinement cycle produced a converged solution, the augmentation factor of the FANTAIL, which is defined as the ratio of the total thrust to the rotor thrust, and which is a key ducted-fan property, did not match well with experiment. Note that for the hovering FANTAIL, the augmentation factor is a particularly useful attribute for validating computational results because it is fairly constant for a wide range of thrust. (see Ref. 5, Fig. 16.) Additional refinement of the grids on the inner shroud (Fig. 5) significantly improved the correlation of the computed augmentation factor with experiment. In Table 2, the refined 1 grid described earlier is compared with the refined 2 grid, which produced a solution with a more accurate augmentation factor. In Fig. 10, the augmentation factors for the two refined grids are compared with the experimental results. As will be illustrated shortly, the likely reason the second grid refinement cycle improved the augmentation factor is that it strengthened the blade tip vortices, thereby increasing the flow through the duct, which simultaneously increased the suction on the shroud lip and reduced the blades' lift.

D. Hovering FANTAIL Results

1. *Flow Description*

Figure 11 shows the velocity field at midazimuth. Qualitatively, the flow closely conforms to expectations: The flow is effectively stagnated beneath the shroud, whereas accelerated flow is visible over the shroud's lip and on the blade tip vortices; note that pressure differences between the lip and underside of the shroud are what generate the shroud thrust. High-speed flow through the central part of the duct is separated by a combination of a shear layer and a blade tip vortex sheet from the stagnated flow under the shroud. The coinciding of the tip vortex sheet with the second grid refinement

Table 2 Grid dimensions, second grid refinement cycle

Grid	Refined 1 grid	Refined 2 grid
Blades	$2 \times (203 \times 40 \times 66) = 1{,}071{,}840$	$2 \times (203 \times 40 \times 66) = 1{,}071{,}840$
Tip caps	$2 \times (148 \times 79 \times 59) = 1{,}379{,}656$	$2 \times (148 \times 79 \times 59) = 1{,}379{,}656$
Root caps	$2 \times (82 \times 73 \times 63) = 754{,}236$	$2 \times (82 \times 73 \times 63) = 754{,}236$
Hub	$111 \times 72 \times 40 = 319{,}680$	$111 \times 72 \times 40 = 319{,}680$
Shroud	2,306,752	$241 \times 299 \times 102 + 105 \times 152 \times 56 = 8{,}243{,}778$
Shroud patches	$2 \times (101 \times 85 \times 44) = 755{,}480$	$2 \times (101 \times 85 \times 75) = 1{,}287{,}750$
Total near body	6,557,292	13,056,940
Off body	3,687,086	3,687,086
Total	10,274,730	16,744,026

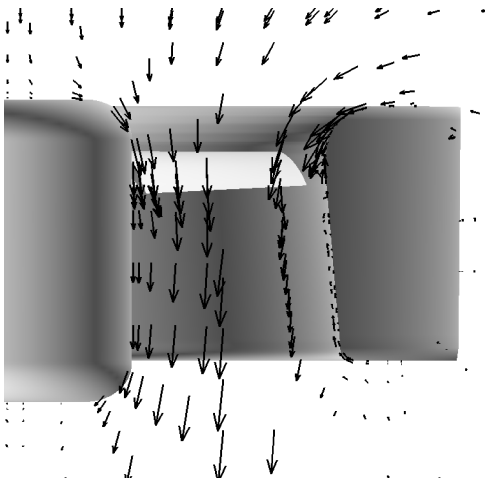

Fig. 11 OVERFLOW-D FANTAIL velocity vectors at midazimuth: hover, 28-deg collective.

region (Fig. 5), coupled with the counterclockwise spin of the vortices, support the contention made earlier that the second grid refinement improved the augmentation factor by strengthening the vortices.

Figure 12 shows a comparison of the velocity field near the duct wall at midazimuth in both the nominal gap and sealed gap configurations. In the nominal configuration, there is upwash, that is, reverse flow, along the duct wall beneath the blades, and close examination reveals that even the small vertical velocity component in the flow beneath the shroud is directed upward. The upwash is induced by the counterclockwise blade tip vortices. Sealing the blade–shroud gap essentially eliminating the upwash, although vortices are still present on the shroud because of shedding from the shroud lip.

The role of tip vortices in the flowfield is further illustrated in Fig. 13, which shows the out-of-plate vorticity measure at midazimuth. Note that a higher collective has been used here to better show the flow's features. Figure 13 clearly reveals the vortex structure of the flowfield, with root vortices plainly visible on the hub, blade tip vortices plainly visible on the shroud, and trailing vortices visible along the length of the blade.

It was noted earlier that sharp flow gradients, and quite possibly convergence considerations, mandate high grid refinement in the blade tip regions. The severity of those gradients is illustrated in Fig. 14, which presents two views of the pressure distribution on the inner shroud surface. Figure 14a shows the steep gradients in the blade–shroud gap areas, which are immediately apparent. Figure 14b shows the pressure coefficient on the shroud just above the blades. The suction peaks within the narrow gaps are caused by air being forced through the gaps under the influence of the sharp pressure jumps between the upper and lower blade surfaces. The pressure jumps near the blade leading edges in Fig. 14b are caused by the same phenomenon: They are not caused by shocks. Thus, significant grid refinement in the blade–shroud gaps would be amply justified on accuracy grounds alone, even if there were no concerns about solution convergence.

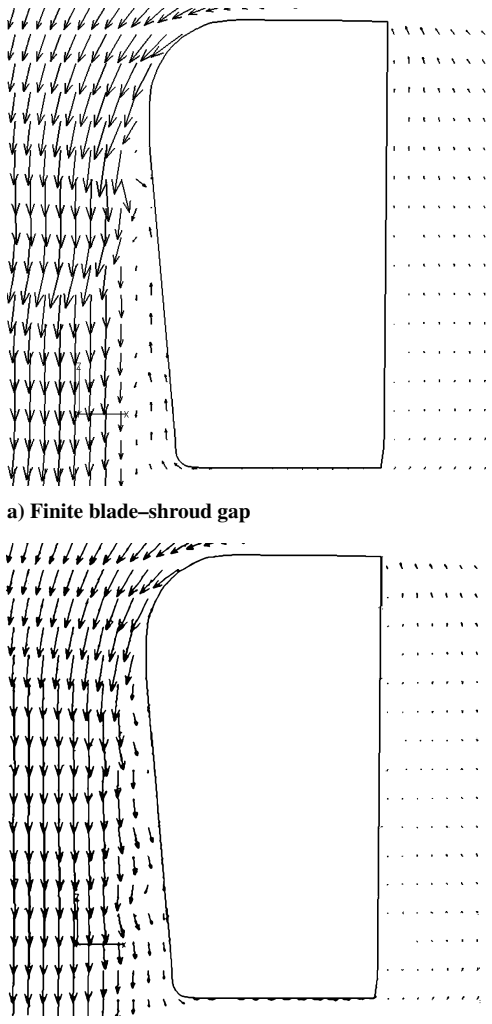

a) Finite blade–shroud gap

b) Sealed blade–shroud gap

Fig. 12 OVERFLOW-D FANTAIL shroud velocity profile: hover, 28-deg collective.

2. Blade Section Lift Forces

Figure 15 shows blade section lift force vs radius for several collective angles. Figure 15 shows that the maximum lift is reached at about 98%R, compared with between 80%R and 90%R for isolated rotor blades. The reason the maximum lift occurs farther out is that the shroud suppresses radial flow, thereby keeping the flow effectively two-dimensional until quite close to the blade tip.

3. FANTAIL Performance

Rotor performance is often assessed by comparing thrust vs power. Figure 16 shows C_q vs $C_t^{3/2}$ from OVERFLOW-D and from the whirl-tower experiment. Note that the agreement between the experimental and computed results is generally good, with the thrust slightly underpredicted for a given torque. Insight into the how the forces are distributed between the rotor and shroud may be gleaned

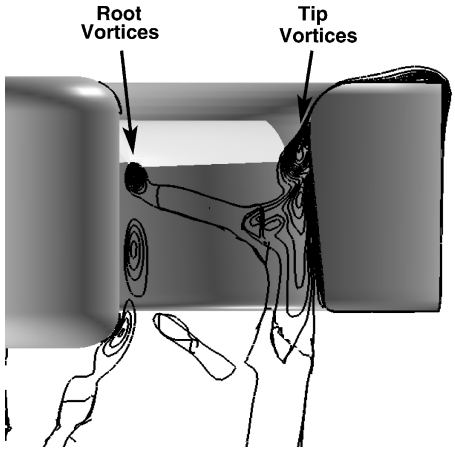

Fig. 13 OVERFLOW-D FANTAIL out-of-plane vorticity profile: hover, 38-deg collective.

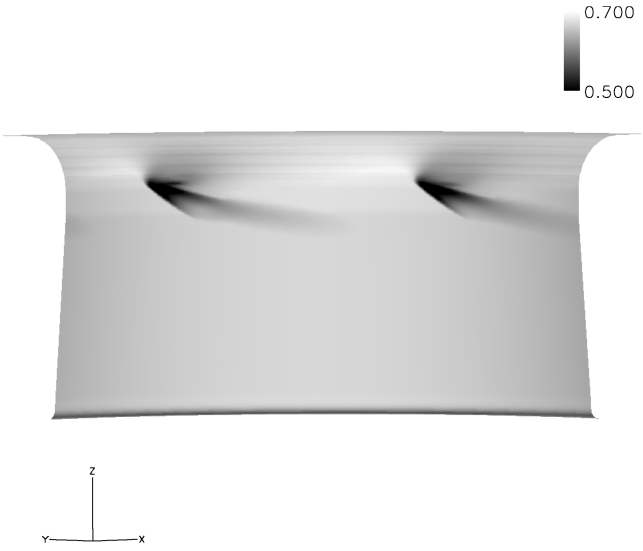

a) Inner duct wall pressure contours

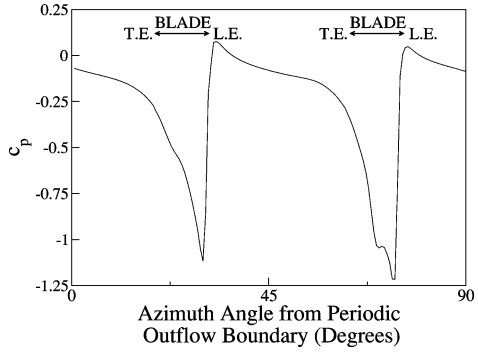

b) Pressure coefficient above rotor disk

Fig. 14 OVERFLOW-D FANTAIL shroud pressure distribution: hover, 38-deg collective.

from the shroud pressure distribution, as in Fig. 17, which shows the shroud pressure coefficient above the rotor disk. The shroud pressures qualitatively match experiment, but are noticeably higher. However, as noted earlier, matching computational and experimental results at a given collective can be problematic because of uncertainties in the experimental blade collective. The total thrust-power results are often found to be more reliable in assessing the accuracy of rotor-related computations because they are less sensitive to such experimental uncertainities.

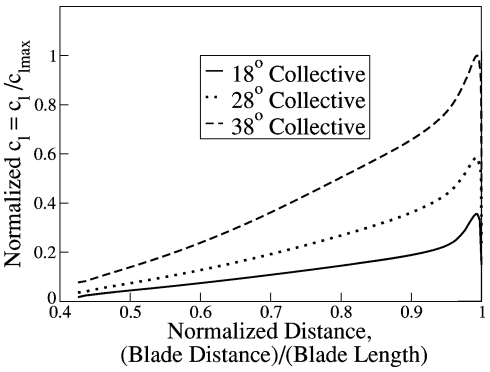

Fig. 15 OVERFLOW-D FANTAIL blade section lift distribution: hover, 18-, 28-, and 38-deg collectives.

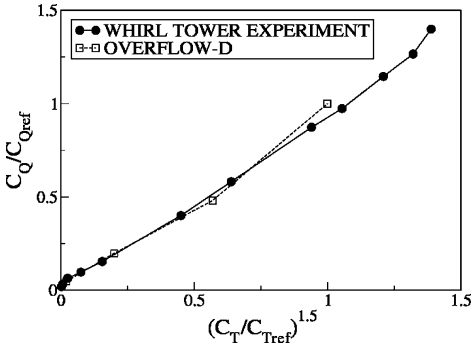

Fig. 16 FANTAIL thrust-power comparison, hover.

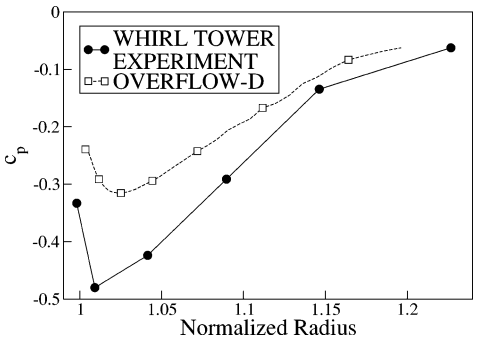

Fig. 17 OVERFLOW-D and experimental FANTAIL pressures on shroud lip: hover, 38 -deg collective.

VI. Conclusions

The Navier–Stokes overset grid flow solver OVERFLOW-D has been successfully adapted to ducted-fan flow using a formulation that satisfies the dual requirements of relative blade–shroud motion and steady solution. The code has been used to compute flow around the RAH-66 FANTAIL, and it has been shown that adequate grid refinement in the vicinity of the blade–shroud gap is crucial in obtaining a converged solution and for resolving key flow details within the gap. The thrust-power predictions show good agreement with experiment, and the solution visualizations demonstrate that reverse flow under the rotor is the result of blade tip vortices rather than duct divergence. The solutions also show that the boundary conditions used on the duct wall can have a profound impact on the flowfield.

Acknowledgments

The authors thank Arsenio C. Dimanlig and Mark A. Potsdam of the U.S. Army/NASA Rotorcraft Division at NASA Ames Research Center for their assistance with running the OVERFLOW-D software. The authors benefitted from discussions with Thomas H. Pulliam of NASA Ames Research Center on the impact of grid refinement on solution convergence and accuracy. The derivation

of the boundary conditions on the duct wall confirmed an earlier, independent study by Arsenio C. Dimanlig and was reviewed by Lakshmi N. Sankar of the Georgia Institute of Technology. Charles Keys, Roger Lacy, and Peter Christis of The Boeing Company provided valuable encouragement and support for using computational fluid dynamics (CFD) methods to model the FANTAIL. Valuable discussions were held with Ganesh Rajagopalan of Iowa State University on FANTAIL modeling using CFD.

References

[1]Rajagopalan, R. G., and Keys, C. N., "Detailed Aerodynamic Design of the RAH-66 Fantail Using CFD," *Journal of the American Helicopter Society*, Vol. 43, No. 4, 1997, pp. 310–320.

[2]Nygaard, T. A., Dimanlig, A. C., and Meadowcroft, E. T., "Application of a Momentum Source Model to the RAH-66 Comanche FANTAIL™," American Helicopter Society, Alexandria, VA, Jan. 2004.

[3]Strawn, R. C., and Djomehri, M. J., "Computational Modeling of Hovering Rotor and Wake Aerodynamics," *Journal of Aircraft*, Vol. 39, No. 5, 2002, pp. 786–793.

[4]Potsdam, M. A., and Strawn, R. C., "CFD Simulations of Tiltrotor Configurations in Hover," American Helicopter Society, Alexandria, VA, June 2002.

[5]Keys, C. N., Sheffler, M., Weiner, S., and Heminway, R., "LH Wind Tunnel Testing: Key to Advanced Aerodynamic Design," American Helicopter Society, Alexandria, VA, May 1991.

[6]Yao, J., Jameson, A., and Alonso, J. J., "Development and Validation of a Massively Parallel Flow Solver for Turbomachinery Flows," AIAA Paper 2000-0082, Jan. 2000.

[7]Vuillet, A., and Morelli, F., "New Aerodynamic Design of the Fenestron for Improved Performance," *12th European Rotorcraft Forum*, Deutsche Gesellschaft für Luft- und Raumfahrt e.V. (DGLR), Bonn, Sept. 1986.

[8]"BVWT 0345: Wind Tunnel Test on the 0.75 Scale L.H.X. Fan-in-Fin Powered Model," The Boeing Co., Rept. 8-7891-1-882, March 1990.

[9]"RAH-66 Demonstration/Validation Fantail Rotor Whirl Test Report," The Boeing Co., Boeing–Sikorsky Document 2000-224-001, Nov. 1996.

[10]Buning, P. G., Jesperson, D. C., Pulliam, T. H., Chan, W. M., Slotnick, J. P., Krist, S. E., and Renze, K. J., "OVERFLOW User's Manual, Version 1.8g," NASA Langley Research Center, Hampton, VA, March 1999.

[11]Holmes, D. G., and Tong, S. S., "A Three-Dimensional Euler Solver for Turbomachinery Blade Rows," *Journal of Engineering for Gas Turbines and Power*, Vol. 107, No. 2, 1985.

[12]Chen, C. L., McCroskey, W. J., and Obayashi, S., "Numerical Solutions of Forward-Flight Rotor Flows Using an Upwind Method," *Journal of Aircraft*, Vol. 28, No. 6, 1991.